Modeling the calibration pipeline of the Lytro camera for high quality light-field image reconstruction

Donghyeon Cho Minhaeng Lee Sunyeong Kim Yu-Wing Tai
Korea Advanced Institute of Science and Technology (KAIST)

Abstract

Light-field imaging systems have got much attention recently as the next generation camera model. A light-field imaging system consists of three parts: data acquisition, manipulation, and application. Given an acquisition system, it is important to understand how a light-field camera converts from its raw image to its resulting refocused image. In this paper, using the Lytro camera as an example, we describe step-by-step procedures to calibrate a raw light-field image. In particular, we are interested in knowing the spatial and angular coordinates of the micro lens array and the resampling process for image reconstruction. Since Lytro uses a hexagonal arrangement of a micro lens image, additional treatments in calibration are required. After calibration, we analyze and compare the performances of several resampling methods for image reconstruction with and without calibration. Finally, a learning based interpolation method is proposed which demonstrates a higher quality image reconstruction than previous interpolation methods including a method used in Lytro software.

1. Introduction

In conventional cameras, we capture a 2D image which is a projection of a 3D scene. In light-field imaging system, we capture not only the projection in term of image intensities but also the directions of incoming lighting that project onto an image sensor. Light-field models the scene formation using two parallel planes, i.e. st plane and uv plane as shown in Figure 1(Left). Coordinates in the st and uv planes represent the intersection of incoming light from different view perspectives and we denote it as $L(s,t,u,v)$. Using this representation, many applications such as refocusing[17, 16], changing view point[11, 10], super-resolution[3, 8, 10, 15, 21, 2], and depth map estimation[1, 6, 4, 20] can be achieved.

In practice, light field images captured by a light field camera are not perfect. Due to manufacturing defection, it is common to have a micro-lens array that does not perfectly align with image sensor coordinates. Blindly re-sample a RAW image into $L(s,t,u,v)$ can be easily caused color shift and rippled like artifacts which can hammer the performances of many post-processing applications. To accurately convert a light field raw image into the representation in $L(s,t,u,v)$ requires careful calibration and resampling. In this paper, using the Lytro camera as an example, we describe step-by-step procedures to calibrate and to convert the raw image into $L(s,t,u,v)$ representation. Although this is a reverse engineering of existing Lytro software, we demonstrate how we can further improve the resulting image in $L(s,t,u,v)$ through a better resampling algorithm.

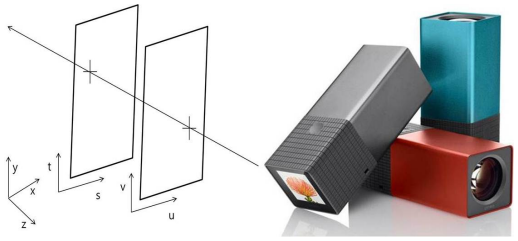

Figure 1. Left: Two planes parameterizations of light field. Right: a Lytro camera.

While this paper was under review, Dansereau *et al*. [7] simultaneously developed a toolbox to decode, calibrate, and rectify lenselet-based plenoptic cameras. However their reconstructed lightfield images have low resolution, e.g. 380×380. In contrast, we demonstrate better and higher resolution, e.g. 1080×1080, lightfield image reconstruction through a better resampling strategy.

To summarize, our contributions are as follows:

1. We model the calibration pipeline of the Lytro light-field camera and describe step-by-step procedures to achieve accurate calibration.
2. We analyze and evaluate several interpolation techniques for pixel resampling in $L(s,t,u,v)$. We show that direct interpolation in RAW images for hexagonal grid produces better interpolation than first making a low resolution regular grid image followed by interpolation.
3. A dictionary learning based interpolation technique is proposed which demonstrates a higher quality image

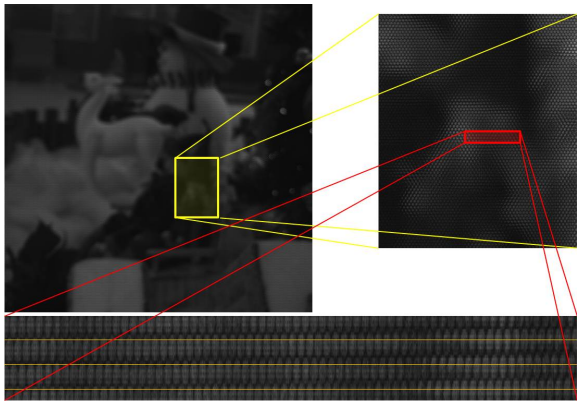

Figure 2. The raw image from Lytro image and enlarged one. Note the micro lens array is not parallel to image coordinate.

reconstruction than previous interpolation methods including method used in Lytro software.

2. Related Works

Recent works that are the closest to ours are reviewed in this section. Since Ng *et al*. [17] presented the prototype light-field camera utilizing micro lens array, many progresses have been made in plenoptic camera developments [19, 12, 13, 18, 14, 5, 7]. A major application of light field camera is the post-digital refocusing which changes focus on a image after a picture is taken. The drawback of such a system, however, is the low resolution that the final images have. To overcome this limitation, many light field super-resolution algorithms have been developed [2, 3, 8, 13, 10].

In [16], Nava *et al*. use ray tracing in light field to get a high resolution focal stack image. They utilize light ray from different direction to obtain sub-pixel details. To render a high resolution image from a micro-lens image, Lumsdaine *et al*. [12, 13] consider the trade off between spatial and angular information in light field capturing. They developed the focused plenoptic camera called plenoptic 2.0 which places the micro lens array behind the main lens image plane and with a small distance in front of image sensor. The plenoptic 2.0 camera sacrifices angular resolution, i.e. u-v plane, to increase spatial resolution, i.e. s-t plane. In [8], Georgiev *et al*. shows a super-resolution algorithm using a plenoptic 2.0 camera to further enhance spatial resolution.

There are also works that utilize light field representation for super-resolution which is independent of hardware configuration knowledge. In [2, 3], Bishop and Favaro analyze the epipolar plane of light-field for depth map estimation and then use deconvolution to reconstruct super-resolution image from micro-lens image. In [21], Wanner and Goldluecke propose a variational model to increase spatial and angular of light-field by utilizing the estimated depth map

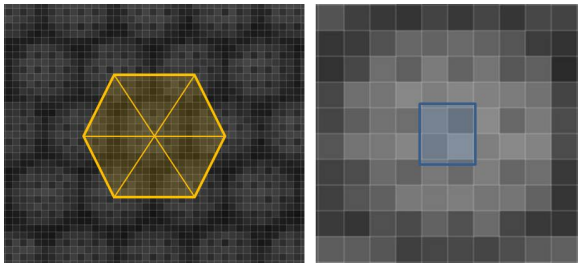

Figure 3. Left: Micro lenses are arranged in hexagonal shape, Right: One micro-lens image.

from EPI image. Levin *et al*. [10] suggest a dimensionality gap prior in the 4D frequency domain of light field for view synthesis and to enhance resolution through frequency domain interpolation without using depth information.

The aforementioned super-resolution algorithms demonstrated high quality super-resolution. Among the discussed techniques, many of them are built on the $L(s,t,u,v)$ representation with regular grid. As noted in our introduction, although the performance of their algorithms highly depends on the process to convert a light-field RAW image to the $L(s,t,u,v)$ representation, not many works have described the conversion procedures systematically. Some of the works assume their initial input is from the light field $L(s,t,u,v)$ representation. In this paper, we systematically analyze the quality of RAW images from the Lytro camera and describe step-by-step procedures to convert RAW to $L(s,t,u,v)$. In our experiments, we also demonstrate different sampling methods that can abruptly affect the quality of the reconstructed $L(s,t,u,v)$. To this end, a dictionary learning based interpolation method is presented for high quality light field image reconstruction.

3. RAW data analysis and calibration

In this section, we analyze the RAW data from the Lytro camera and describe our calibration procedures to correct the misalignment error between micro lens array and image sensor. In the next section, we evaluate different resampling methods and propose our learning based interpolation method for high quality light field image reconstruction.

3.1. Raw Data Analysis

After an image is captured by the Lytro camera, the RAW data is stored in their $.lfp$ file format. The $.lfp$ file contains camera parameters such as focal length in the file header and a RAW image file as shown in Figure 2. The RAW image file is a gray-scale image with 'BGGR' Bayer pattern to store values of different RGB channels. The resolution of the RAW image has 3280×3280 pixels and it stores 12-bits per pixel. The micro lens array in a Lytro camera has a hexagonal shape arrangement as shown in Figure 3 instead of a grid arrangement which has smaller gaps be-

Algorithm 1 Calibration Procedures

Capture multiple white RAW images
Gamma correction
Compute Average White Images (Figure 4(a))
Demosaicking (Figure 4(b))
Grayscale image conversion (Figure 4(c))
Contrast stretching (Figure 4(d))

1: **procedure** Rotation Estimation
   Find Local Maxima in the Frequency Domain (Figure 5(a))
   Rotate Image by the Estimated Angle (Figure 5(c))
2: **procedure** Center Pixel Estimation
   Erode Rotated Image (Figure 6(a))
   Find Local Maxima and Fit paraboloid (Figure 6(b))
   Estimate Center Points (Figure 6(c))
   Fit Delaunay Triangulation (Figure 6(d))

tween micro lenses and therefore allows more light rays to be captured. For each micro lens, the diameter is around 10 pixels and the physical size of each micro lens is around $1.4 \times 10^{-5} m$. If we divide the image dimension by the size of micro lens (assuming grid based micro lens array), the effective resolution of the reconstructed light field image is 328×328. However, the rendered refocus image using the Lytro software has a resolution 1024×1024. This implies that the Lytro software has a algorithm to enhance the resolution of rendered images instead of using a naive method to reconstruct a low resolution light-field image for rendering.

3.2. Calibration

In order to convert the RAW image file to the light field image representation effectively, we need to calibrate the RAW image. The main goal of this calibration is to identify center point locations of each micro-lens sub-image and rearrange them in a regular basis for better resampling which will be described in the next section. Our calibration procedure is summarized in Algorithm 1.

To calibrate the RAW image, we capture a white scene such that the captured images should be all white and homogeneous in color. To reduce the effects of sensor noise in calibration, the white images are captured multiple time and we use the average image for our calibration. For each individual capture, we apply Gamma correction to correct intensity where the gamma value can be found in the $.lfp$ header file. Since the captured image is white in color, the color value of RGB channels should be the same and we use it to demosaick the true color image. Next, we convert the RGB image into a Gray scale image and stretch the intensity range so that we can easily process the image in later steps. The intermediate results of these calibration processes are in Figure 4.

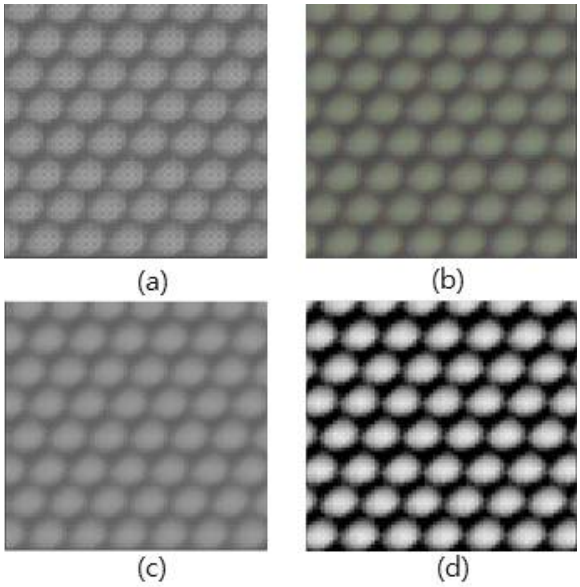

Figure 4. (a) Averaged white raw image, (b) Result of demosaicking and stretching, (c) Gray scale image, (d) Contrast Stretched image.

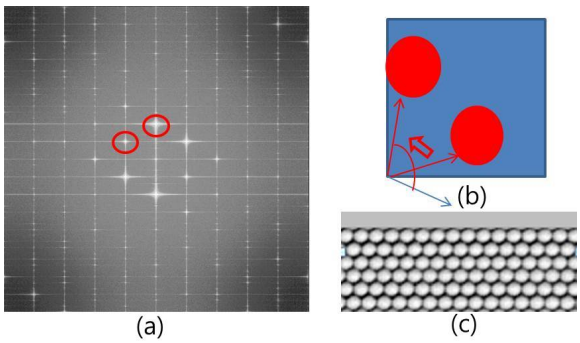

Figure 5. (a) Frequency domain of micro lens image. Note the periodic pattern of coefficients due to the repetition micro lens image. (b) Initial rotation of micro lens image in RAW, (c) Rotation compensated micro lens image.

Our next step is to estimate the rotation of micro lens array to compensate the misalignments between micro lens array and image sensor. We adopt the frequency domain approach to estimate the rotation of the micro-lens array. In the frequency domain, strong periodic components in the spatial domain produce peak value coefficients. We estimate the rotation of micro lens image by looking for a local maxima coefficient closest to the zero frequency location as shown in Figure 5(a). The selected frequency represents the direction that has the most repeated of the periodic patterns, i.e. micro lens image, and hence we get the rotation of micro lens array. Note that if the micro lens array aligns with pixel axis, the peak frequency should be in vertical or horizontal direction, but we barely find such case in our calibration. Using the estimated axes, we rotate the RAW image to align with pixel axis as shown in Figure 5(c).

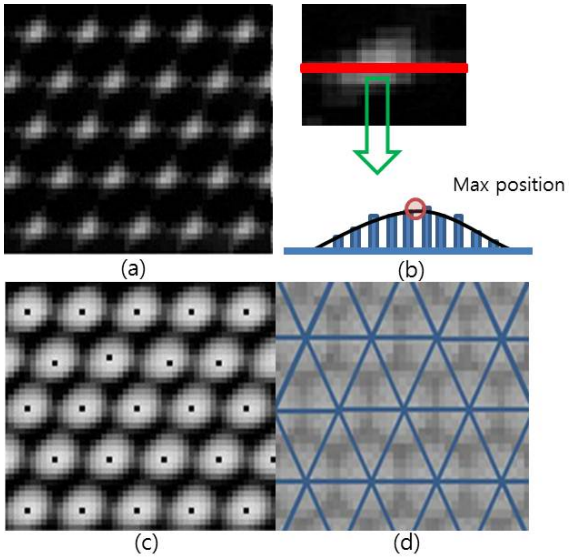

Figure 6. (a) Eroded image, it has max value in center point, (b) paraboloid fitting to find precise local maximum, (c) Estimated center point, (d) Delaunay Triangulation on micro-lens image.

Finally, we estimate the center point of micro lens by applying the eroding operation as shown in Figure 6(a). The non-uniformity of micro-lens center can be due to manufacturing defection where each micro lens have slightly different shape. Because each micro-lens diameter is around 10 pixels, integer pixel unit is not sufficient to represent the exact center points. Thus, we take the sub-pixel unit. To get the sub-pixel precision, we apply the paraboloid fitting to the eroding result as illustrated in Figure 6(b). This is reasonable since the micro-lens array is a 2D periodic paraboloid. Figure 6(c) shows the estimated center points of each micro lens image. Lastly, we use the Delaunay Triangulation to fit a regular triangle grid to the estimated center points of micro lens image and shift the micro lens image locally to obtain our calibrated image. Once we obtain the calibrated parameters, we can apply them to other images captured from the same Lytro camera. Comparing our calibration with Dansereau *et al*. [7], they additionally perform rectification to correct radial distortion, we refer readers to Dansereau *et al*. [7] for the details of the rectification process.

4. Light field image Reconstruction

Using the calibrated data from Section 3.2, we can reconstruct a regular grid light-field image by interpolation. Decoding and rectification methods for Lytro are suggeted in [7]. However, their target resolution for reconstruction is small. In this section, we analyze and evaluate the effectiveness of several interpolation methods and propose our own dictionary learning based interpolation method. Since the resulting image size from Lytro software is 1080×1080, we set the target resolution of our reconstructed light field image to be 1080×1080.

4.1. Downsampling followed by bicubic interpolation

As described in the previous section, the size of a RAW image is 3280×3280 ($> 1080 \times 1080$). However, when taking the diameter of micro lens (10 pixels) into account, the effective resolution is lower than the target resolution. A naive interpolation method is to first downsample the RAW image by a factor of 10 (i.e. diameter of micro lens) to obtain a well sampled low resolution regular grid light field image at a resolution of 328×328. Then, we use bicubic interpolation to upsample the low resolution light field image to the target resolution. We consider this method as the baseline method. In our experimental analysis, this method creates unnatural aliasing due to the downsampling and upsampling processes. In addition, some high frequency details are lost in the downsampled light field image.

4.2. Barycentric interpolation at target resolution

To fully utilize the hexagonal layout of the micro lens array, we resize the triangular grid from the calibrated data to the target resolution. Then, we apply Barycentric interpolation to directly interpolate the pixel values from the micro lens centers at triangle corners. This is given by:

$$I(p) = \lambda_1 I(x_1, y_1) + \lambda_2 I(x_2, y_2) + \lambda_3 I(x_3, y_3), \quad (1)$$

and λ_1, λ_2, and λ_3 can be obtained by solving:

$$\begin{aligned} x &= \lambda_1 x_1 + \lambda_2 x_2 + \lambda_3 x_3 \\ y &= \lambda_1 y_1 + \lambda_2 y_2 + \lambda_3 y_3 \\ 1 &= \lambda_1 + \lambda_2 + \lambda_3 \end{aligned} \quad (2)$$

where p is the center point coordinate, and $I(x_1, y_1)$, $I(x_2, y_2)$, $I(x_3, y_3)$ are the intensity values at the three corners. The Barycentric interpolation produces higher quality interpolation comparing to the previous method since it does not involve any downsampling. Also, the hexagonal layout of the micro lens array gives smoother edges with less aliasing artifacts.

4.3. Refinement using Multiple-Views

The Barycentric reconstruction uses only one pixel per micro lens image to reconstruct the light field image. In order to reconstruct a higher quality light field image, we can use more pixels from each micro lens image for reconstruction. Since pixels in a micro lens image represent rays from slightly different perspectives, we use ray interpolation to find the intercepting point of the ray direction and the current image plane and then copy the color value of rays to the intercepted pixel location.

In order to get the ray direction of each pixel, we analyze the epipolar image as discussed in previous light field

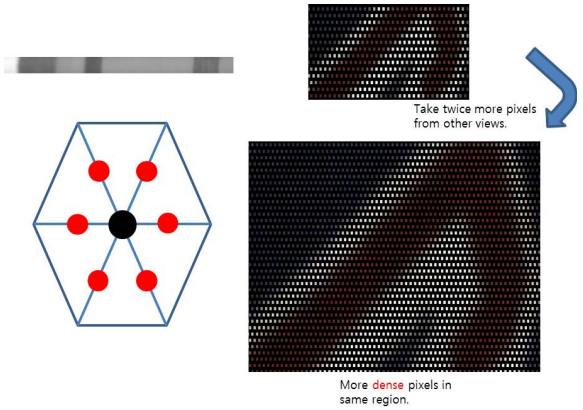

Figure 7. Top left: Epipolar image from the Barycentric reconstruct light field image, Bottom left: Red points are from other view. Top right: Pixels from one view, Bottom right: Pixels from multiple view.

super-resolution techniques [20, 21]. Specifically, the gradient direction in the epipolar image is proportional to the depth of a 3D scene. Once we know the depth, we can apply ray tracing to fill in the pixel values from adjacent views. This method is similar to the method in [16] for making high resolution focal stack images. Figure 7(Top Left) shows an example of epipolar image from the Barycentric reconstruction lightfield image. Figure 7(Bottom Left) illustrates the copied pixels from adjacent views which follow the hexagonal arrangement of micro lens array in the Lytro camera. The increase in number of sampled pixels is illustrated in the Figure 7(Top and Bottom Right). The remaining empty pixels within the triangle area are again interpolated by the Barycentric interpolation. After this multi-view refinement, we obtain more details in the reconstructed light field image.

4.4. Learning based Interpolation

The multi-view refined light field image still contains aliasing which is unnatural. In this section, we adopt a learning based technique to train a dictionary that encodes natural image structures and use it to reconstruct our light field image. Our learning based interpolation is inspired by the work in [22, 9] in which they use dictionary learning with sparse coding to reconstruct super-resolved image from a low quality and low resolution image. To prepare our training data, we use our calibrated Lytro parameter to generate a synthetic triangular grid image by dropping pixel values at the location that were interpolated by the Barycentric interpolation. After that, we use the Barycentric interpolation to re-interpolate the pixel values to get a synthesized image after the multi-view refinement. Using these image pairs, we train a dictionary by solving the following sparse coding equation:

$$\{D_h, D_l\} = \arg\min_{D\alpha} \|D\alpha - T\|_2^2 + \lambda \|\alpha\|_1 \qquad (3)$$

where $D = \{D_h, D_l\}$ is the trained dictionary which consists of high quality and low quality dictionary pair, T is our training examples, and α is the sparse coefficient. We refer reader to [22] for more details about the dictionary learning process. In the reconstruction phase, we estimate the sparse coefficients which can faithfully reconstruct the multi-view refined light field image using the low quality dictionary by solving the following equation:

$$\arg\min_{\phi} \|D_l\phi - I_l\|_2^2 + \lambda \|\phi\|_1 . \qquad (4)$$

Next, we substitute the low quality dictionary with the high quality dictionary and then reconstruct the light field image again using the high quality dictionary and the estimated sparse coefficients. After the learning based interpolation, our reconstructed light field images are of high quality which contains high resolution details without any aliasing.

5. Experimental Results

This section shows our reconstructed light field images from the Lytro RAW data. We examine the effects of the calibration by comparing the reconstructed light-field images with and without the calibration. In our experiment, we reconstruct light field images, $L(s, t, u, v)$, with size 7×7 by using only the pixels around the calibrated center points of micro lens images. This is because the micro lens has vignetting and other non-uniform effects which greatly degrade the reconstructed light field image from the border pixels of micro lens images. Also, 7×7 light field images are already sufficient for post-focusing methods [17, 16] and many light field super-resolution algorithms [3, 8, 10, 15, 21, 2].

Effects on Calibration. We compute the results with and without calibration by assuming the positions of each center pixel of micro lens which are fixed on a given hexagonal grid. We show the reconstructed center view image in Figure 8 for comparisons. As shown in the leftmost column, results without calibration have blur, aliasing and color shift artifacts. This is because the reconstructed images without calibration can contain pixels from other view perspective. After calibration, the aliasing artifacts are reduced and edges are sharper as shown in the center images respectively. For references, we also show the reconstructed center view on the rightmost column after multi-view refinement.

Effects on Sub-pixel precision estimation of center points. We examine the reconstructed center view with and without sub-pixel precision estimation of center points

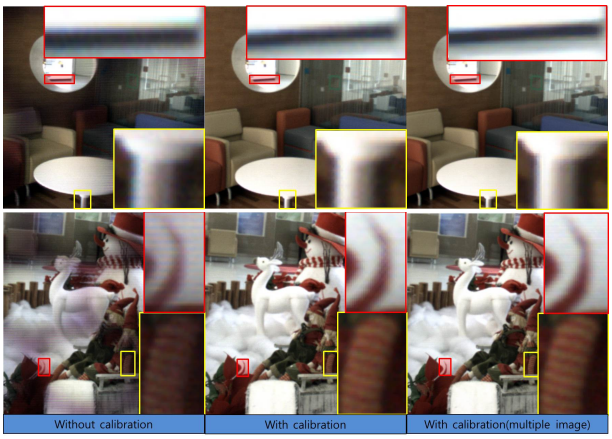

Figure 8. Comparison with results without calibration indoor scene. Left: without calibration, Center: with calibration, Right: multiple images are used with calibration. Results without calibration has many artifacts compared with calibrated results. Multiple images which have different view points make more details.

in Figure 9. Since the micro-lens array does not fully align with image sensors, using the integer pixel unit to represent micro lens centers can cause large errors especially when each of the micro lens is very small. As shown in Figure 9, result without sub-pixel precision estimation shows block artifacts around diagonal edges. In contrary, the results with sub-pixel accuracy of center points has less aliasing artifacts and straighter lines.

Comparisons of different resampling methods

In order to examine the effect on different resampling, we compare the reconstructed center view from the bicubic interpolation method described in Section 4.1, the Barycentric interpolation method described in Section 4.2, the multi-view refinement method described in Section 4.3, and the dictionary learning based interpolation method described in Section 4.4 in Figure 10 and Figure 11.

In Figure 10 (b), blur and aliasing artifacts appear particularly in the edge region of resolution chart because some high frequency details have lost in the downsamping process. The Barycentric reconstruction at the target resolution with downsampling shows distinguishable lines in the resolution chart in Figure 10 (c) and better results in Figure 11. In Figure 8, Figure 10 (d), and the third column of Figure 11, we show the reconstructed results with multi-view refinement which contains more details comparing to single view Barycentric reconstruction method. We also apply learning based interpolation on top of calibration and sub-pixel precision processes. As shown in Figure 11, the learning based result shows the most sharper edges and less jagged artifacts among comparing results. Since a low resolution image is directly replaced by high resolution based on the dictionary, it has less aliasing artifacts, while other results based on the interpolation method still have jagged

Figure 9. Barycentric reconstruction without (Left) and with (Right) sub-pixel precision estimation of micro lens center.

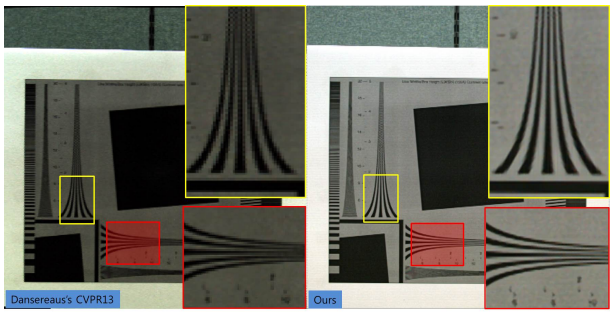

Figure 12. Comparison with Dansereaus *et al*. [7].

lines as clearly seen in the top row. Lastly, we show results from Lytro built-in software in the rightmost column in Figure 11. Comparing the Lytro software results, our multi-view refinement has similar quality reconstruction. We can also see that the dictionary learning interpolation outperforms Lytro software results with more details and less aliasing. Finally, we compare our reconstructed image with the reconstructed image using the toolbox from Dansereau *et al*. [7] in Figure 12. Note that our results are of higher resolution and with more details and less aliasing artifacts.

6. Conclusion and discussion

We have presented the calibration pipeline of Lytro and several resampling algorithms for light field image reconstruction. Although this work is mostly engineering, it gives a good case study to understand the process of calibration and demonstrate the importance of developing better light field reconstruction algorithm for converting RAW to $L(s,t,u,v)$. In the calibration, the Lytro RAW data is converted into the light-field representation $L(s,t,u,v)$ and we estimate the center points in raw data which has a hexagonal formation. Then, we sample the pixels preserving the hexagonal formation. To reconstruct high quality light field images, we design the learning based interpolation algorithm and demonstrate that our learning based algorithm outperforms other resampling methods including results from the Lytro software.

In this paper, we have also shown that the importance of

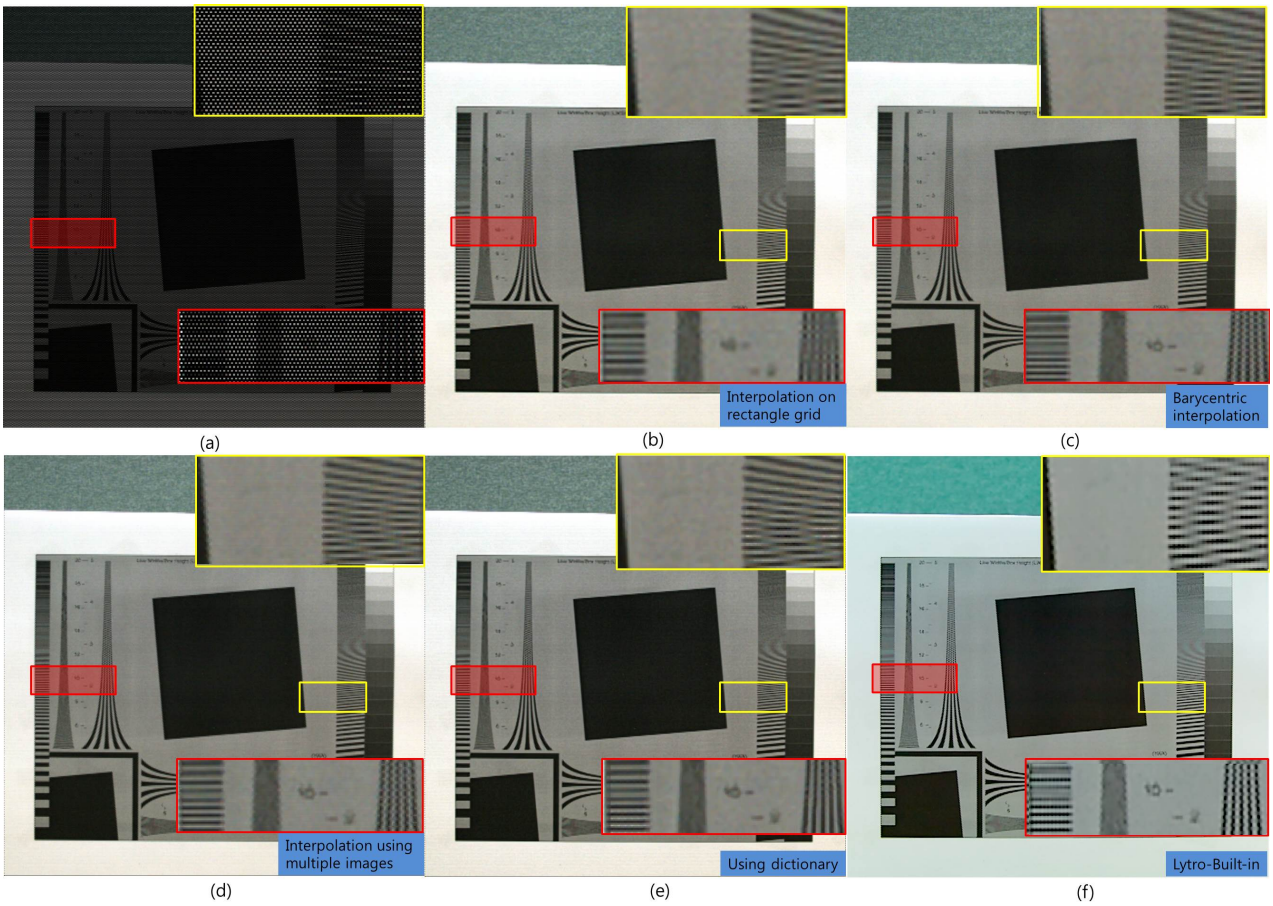

Figure 10. Real world examples using resolution chart. (a) Extracted pixels on hexagonal grid, (b) Bicubic interpolation on low resolution image, (c) Barycentric interpolation, (d) Using multiple images, (e) our learning based method, (f) Lytro built-in.

knowing calibration parameters for high quality light-field reconstruction. While most previous works assume that the light field representation is given from plenotic cameras, the quality of light field images can vary a lot and hence can greatly affect the performances of post-processing algorithms. In the future, we plan to extend our work to combine with other light-field super-resolution algorithms to further enhance the resolution and quality of the light field image.

7. Acknowledgements

We thank the anonymous reviewers for their valuable comments. This research is supported by the KAIST High Risk High Return Project (HRHRP) (N01130151), and the Study on Imaging Systems for the next generation cameras funded by the Samsung Electronics Co., Ltd (DMC R&D center) (IO120712-04860-01).

References

[1] E. H. Adelson and J. Y. A. Wang. Single lens stereo with a plenoptic camera. *IEEE Trans. PAMI*, 14(2):99–106, Feb. 1992. 1

[2] T. E. Bishop and P. Favaro. The light field camera: Extended depth of field, aliasing, and superresolution. *IEEE Trans. PAMI*, 34(5):972–986, 2012. 1, 2, 5

[3] T. E. Bishop, S. Zanetti, and P. Favaro. Light field superresolution. In *IEEE ICCP*, 2009. 1, 2, 5

[4] T. E. Bishop, S. Zanetti, and P. Favaro. Plenoptic depth estimation from multiple aliased views. In *IEEE ICCV Workshops*, 2009. 1

[5] CAVE Laboratory, Columbia University. Focal sweep photography. http://www.focalsweep.com/. 2

[6] D. G. Dansereau and L. T. Bruton. Gradient-based depth estimation from 4d light fields. In *ISCAS*, 2004. 1

[7] D. G. Dansereau, O. Pizarro, and S. B. Williams. Decoding, calibration and rectification for lenselet-based plenoptic cameras. In *IEEE CVPR*, 2013. 1, 2, 4, 6

[8] T. Georgiev and A. Lumsdaine. Superresolution with plenoptic camera 2.0. Technical report, Adobe Systems, 2009. 1, 2, 5

[9] Y. Hitomi, J. Gu, M. Gupta, T. Mitsunaga, and S. K. Nayar. Video from a single coded exposure photograph using a learned over-complete dictionary. In *IEEE ICCV*, 2011. 5

[10] A. Levin and F. Durand. Linear view synthesis using a dimensionality gap light field prior. In *IEEE CVPR*, 2010. 1, 2, 5

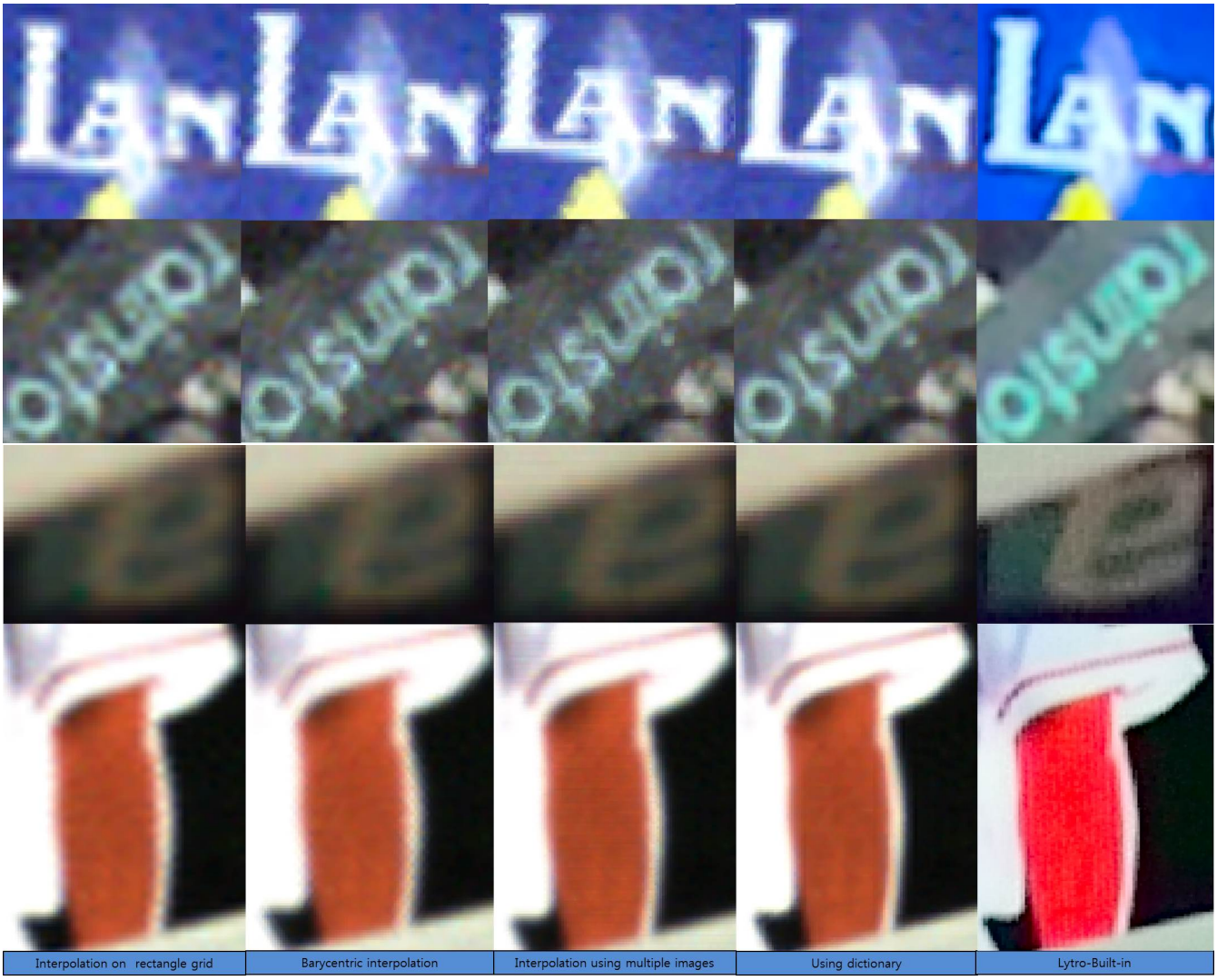

Figure 11. Real world examples. (From left to right) Bicubic interpolation on rectangle grid at low resolution, barycentric interpolation on hexagonal grid, multiple images interpolation, learning based method, Lytro built-in method.

[11] M. Levoy and P. Hanrahan. Light field rendering. In *ACM SIGGRAPH*, 1996. 1

[12] A. Lumsdaine and T. Georgiev. Full resolution lightfield rendering. Technical report, Technical report, Adobe Systems, 2008. 2

[13] A. Lumsdaine and T. Georgiev. The focused plenoptic camera. In *IEEE ICCP*, 2009. 2

[14] Lytro. The lytro camera. https://www.lytro.com. 2

[15] K. Mitra and A. Veeraraghavan. Light field denoising, light field superresolution and stereo camera based refocussing using a gmm light field patch prior. In *IEEE CVPR Workshops*, 2012. 1, 5

[16] F. P. Nava and J. P. Luke. Simultaneous estimation of superresolved depth and all-in-focus images from a plenoptic camera. In *3DTV Conference*, 2009. 1, 2, 5

[17] R. Ng, M. Levoy, M. Brédif, G. Duval, M. Horowitz, and P. Hanrahan. Light field photography with a hand-held plenoptic camera. Technical report, 2005. 1, 2, 5

[18] Raytrix. 3d light field camers. http://raytrix.de/. 2

[19] A. Veeraraghavan, R. Raskar, A. Agrawal, A. Mohan, and J. Tumblin. Dappled photography: Mask enhanced cameras for heterodyned light fields and coded aperture refocusing. *ACM Trans. on Graphics*, 26(3), 2007. 2

[20] S. Wanner and B. Goldlücke. Globally consistent depth labeling of 4d light fields. In *IEEE CVPR*, 2012. 1, 5

[21] S. Wanner and B. Goldluecke. Spatial and angular variational super-resolution of 4d light fields. In *IEEE ECCV*, 2012. 1, 2, 5

[22] J. Yang, J. Wright, Y. Ma, and T. Huang. Image superresolution as sparse representation of raw image patches. In *IEEE CVPR*, 2008. 5